Interplay among spin, orbital, and lattice degrees of freedom in a frustrated spinel Mn_3O_4

Y. Nii,[1,2] H. Sagayama,[2] H. Umetsu,[1] N. Abe,[2] K. Taniguchi,[3] and T. Arima[2]
[1]*Institute of Multidisciplinary Research for Advanced Materials, Tohoku University, Sendai 980-8577, Japan*
[2]*Department of Advanced Materials Science, University of Tokyo, Kashiwa 277-8561, Japan*
[3]*Department of Physics, University of Tokyo, Bunkyo, Tokyo 113-0033, Japan*
(Received 22 February 2013; published 13 May 2013)

We have investigated magnetic-field ($H \| [100]$) effect on a spin-frustrated tetragonally distorted spinel Mn_3O_4 by measurements of magnetization, dielectric constant, and strain as well as synchrotron x-ray and neutron diffraction. In two low-temperature phases below 40 K, long-wavelength lattice modulations coupled with magnetic order have been confirmed, revealing spin-lattice coupling caused by the exchange striction in the geometrically frustrated Mn^{3+} spin moments on the distorted pyrochlore lattice. A magnetic-field-induced phase transition has been found at low temperatures, which involves an abrupt change in both structural and magnetic configurations. The magnetostructural phase transition by the application of a magnetic field $H \| [100]$ is discussed in terms of interplay among spin, orbital, and lattice degrees of freedom.

DOI: 10.1103/PhysRevB.87.195115 PACS number(s): 75.25.−j, 75.25.Dk, 71.70.Ej, 75.80.+q

I. INTRODUCTION

Spinel oxides with a general formula AB_2O_4 have provided a good arena for studying the effects of geometrical frustration and a coupling among spin, orbital, and lattice degrees of freedom.[1] The geometrical frustration arises when magnetic moments at the B sites, which form a three-dimensional network of corner-sharing tetrahedra referred to as pyrochlore lattice, antiferromagnetically interact with each other. In the frustrated magnet, an external stimulus may lead to a drastic variation of physical properties via a change among highly degenerate manifold states. For example, Mn_3O_4 exhibits a variety of physical phenomena, such as magnetodielectric,[2,3] magnetoelastic,[3] and magnetocaloric[4] behaviors, and a quantum phase transition.[5,6] In Mn_3O_4, the tetrahedral A sites and octahedral B sites are selectively occupied by Mn^{2+} and Mn^{3+} ions, respectively [Fig. 1(a)].[7,8] Twofold orbital degeneracy in the e_g level at each B site Mn^{3+} leads to a cooperative Jahn-Teller transition far above room temperature ($T_{JT} = 1443$ K). The $|3z^2 - r^2\rangle$ ferro(F) orbital order at T_{JT} induces a huge tetragonal distortion ($c/a \sim 1.16$).[2,9,10] Consequently, there is no orbital degeneracy in Mn_3O_4 below T_{JT}.

It was reported that Mn_3O_4 exhibits successive phase transitions in the absence of a magnetic field from paramagnetic (PM) to Yafet-Kittel (YK) phase at $T_N = 42$ K, then to an incommensurate (IC) phase at $T_1 = 40$ K, and finally to a commensurate phase, called cell-doubled (CD) phase, at $T_2 = 34$ K.[2] Moreover, recent precise measurements of heat capacity and magnetization revealed a new anomaly at $T^* = 38$ K.[11] These complicated magnetic phase transitions are indicative of magnetic frustration in the tetragonal spinel Mn_3O_4. In the YK and the CD phases, the Mn^{2+} spins align ferromagnetically along [110], while the net of Mn^{3+} spins is antiparallel to Mn^{2+} spins,[12,13] where the antiferromagnetic (AF) coupling between neighboring Mn^{3+} spins and the single-ion anisotropy (easy axis along the c axis) of each Mn^{3+} spin result in a triangular spin configuration, as shown in Fig. 1(b). In this paper, the crystal axis is represented not in the body-centered tetragonal setting but in the face-centered tetragonal setting in order to avoid the transformation of the crystal axis directions across a tetragonal-to-face-centered-orthorhombic phase transition, discussed later. The YK phase is a coplanar ferrimagnet without a magnetic superlattice, while long-wavelength magnetic modulations are present in the IC and CD phases.[12,13] The CD phase has a magnetic unit cell doubled along the [110] axis.[3] Recently, Kim *et al.* reported that the crystallographic symmetry of the CD phase is lowered from tetragonal to body-centered-orthorhombic structure, with the principle axes of [001], [110], and $[1\bar{1}0]$.[5,6]

According to a previous inelastic neutron scattering measurement, the Jahn-Teller-driven gigantic tetragonal distortion makes the exchange interaction between in-plane nearest neighbor Mn^{3+} ions J_{BB} much stronger than that between out-of-plane nearest neighbor Mn^{3+} ions J'_{BB}, in Fig. 1(c) ($|J'_{BB}|/|J_{BB}| \sim 0.06$).[14] Here, J_{BB} is also stronger than the AF interaction between neighboring A and B sites (J_{AB}) : $|J_{AB}|/|J_{BB}| \sim 0.11$.[14] Due to the predominant J_{BB}, Mn^{3+} spins tend to form one-dimensional (1D)-AF chains along [110] or $[1\bar{1}0]$. As a consequence, the B sites in Mn_3O_4 can be regarded as a stacking of 1D-AF chains, mutually coupled via weak J'_{BB}. Although the formation of 1D-AF chains can partly relax the magnetic frustration, the degeneracy with respect to the relative phases of 1D-AF chains still remains. Considering the c axis components of B-site Mn^{3+} moments, the main difference between YK and CD phases is a stacking pattern of frustrated 1D-chains. It implies that the magnetic transitions in Mn_3O_4 should be understood in terms of rearrangements in the stacking of 1D-AF chains.

Anisotropic magnetoelastic[3] and magnetodielectric[2,3] behaviors were observed in Mn_3O_4 when a magnetic field was applied along [100]. These effects are explained by the modulation of Mn^{3+} orbital states through the inverse process of single-ion spin anisotropy[3] or by spin-phonon coupling.[2] Note that these responses for $H \| [100]$ are not considered to correspond to a tetragonal-to-orthorhombic phase transition induced by a magnetic field along [110] reported by Kim *et al.*[5] When a magnetic field is applied along [110], elongation (compression) takes place along [110] ($[1\bar{1}0]$), while the application of a magnetic field along [100] induces elongation (compression) along [100] ([010]).[3] Thus, drastic changes in elastic and dielectric properties in $H \| [100]$ suggest another

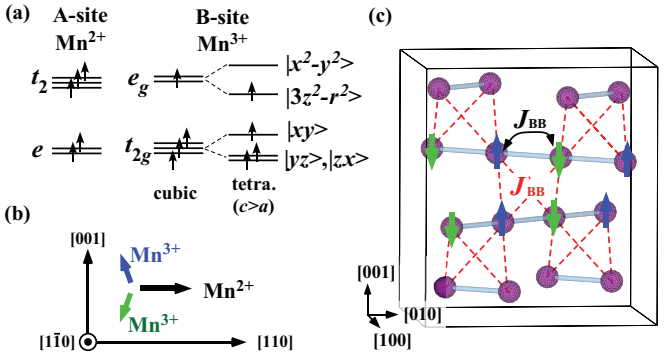

FIG. 1. (Color online) (a) Energy levels of tetrahedral A-site Mn^{2+} and octahedral B-site Mn^{3+} in Mn_3O_4. The orbital degree of freedom at B-site Mn^{3+} is lifted by a gigantic elongation along the c axis below a cubic-tetragonal phase transition temperature. (b) Schematic view of spin arrangements in YK and CD phases. The A-site Mn^{2+} and B-site Mn^{3+} forms YK-type triangular spin configuration on $(1\bar{1}0)$ plane. (c) Formation of 1D-AF chains of B-site Mn^{3+} ions along [110] and $[1\bar{1}0]$ due to the dominant exchange J_{BB}. There still remains magnetic frustration about how to stack the antiferromagnetic chains via an interchain interaction (J'_{BB}).

type of structural phase transition, and which may also involve a rearrangement of frustrated 1D-AF chains, that has not been reported so far. Here, we focus on the magnetic-field-induced phase transition of Mn_3O_4 in a magnetic field along [100]. The phase transition is investigated by magnetization, dielectric constant, and strain combined with synchrotron x-ray and neutron diffraction measurements. The present study reveals that the interplay among spin, orbital, and lattice degrees of freedom results in a rearrangement of frustrated 1D-AF chains and causes the magnetoelastic and the magnetodielectric responses in Mn_3O_4.

II. EXPERIMENT

Single crystals of Mn_3O_4 were grown by a floating-zone method. X-ray Laue photographs were used to determine the crystallographic orientation. Magnetization was measured by a superconducting quantum interference device magnetometer. The strain measurements in a magnetic field along [100] were performed by a conventional strain gauge technique. For the measurement of dielectric constant ε at 10 kHz along [100], gold electrodes were sputtered on two wide (100) faces of a thin-plate crystal. The ε measurement was performed in a magnetic field along [100] using an LCR meter (4263B; Agilent Co. Ltd.) at the High Field Laboratory for Superconducting Materials, Institute for Materials Research, Tohoku University, Japan. Synchrotron x-ray diffraction measurements were performed on BL-3A at Photon Factory, KEK, Japan. The x-ray beam was monochromatized to 12 keV using a Si (111) double-crystal. A single crystal was attached to an aluminum plate and mounted with the [010] axis parallel to the scattering vector. An external magnetic field was applied along [100] by using a split-type superconducting magnet. Neutron scattering measurements were carried out by using the Polarized Neutron Triple-Axis Spectrometer (PONTA) on 5G at JRR-3, Japan. Thermal neutron beam was monochromatized to $E_i = 80.0$ meV using a pyrolytic graphite. A single-crystalline sample was mounted in a split electromagnet in order to apply a magnetic field along [100].

III. RESULTS AND DISCUSSIONS

A. Magnetization, dielectric constant, and strain

Figure 2 shows temperature dependence of magnetization M, dielectric constant $\Delta\varepsilon/\varepsilon$, and strain $\Delta L/L$ along [100] in various magnetic fields applied along [100]. As the temperature decreases, the magnetization increases at the onset of the YK phase. We observed another small increase in M at the lower temperature. The anomaly shifts to a higher temperature with an increasing magnetic field. The dielectric constant steeply decreases, while the strain steeply increases upon cooling, being consistent with the previous report by Suzuki *et al.*[3] We found that the lower-temperature anomaly in M corresponds to the drastic changes in $\Delta\varepsilon/\varepsilon$ and $\Delta L/L$. These coincident responses in M, $\Delta\varepsilon/\varepsilon$, and $\Delta L/L$ in a magnetic field are indicative of a phase transition, which may involve a variation of both magnetic and structural configurations. Figure 2(d) shows strain as a function of a magnetic field along [100] at 5 K. In the ab plane, the lattice is elongated

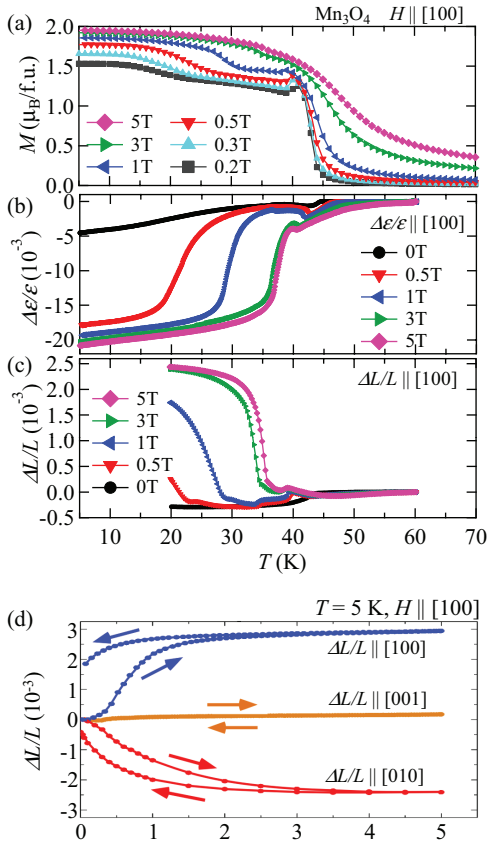

FIG. 2. (Color online) Temperature dependence of (a) magnetization, (b) dielectric constant, and (c) strain under various magnetic field strengths. The measurements were performed upon cooling in a magnetic field along [100]. The relative changes in the dielectric constant and the strain are defined as $\Delta\varepsilon/\varepsilon = \{\varepsilon(T) - \varepsilon(60\text{ K})\}/\varepsilon(60\text{ K})$ and $\Delta L/L = \{L(T) - L(60\text{ K})\}/L(60\text{ K})$. (d) Magnetic-field dependence of strain along [100], [010], and [001] at 5 K in a magnetic field along [100].

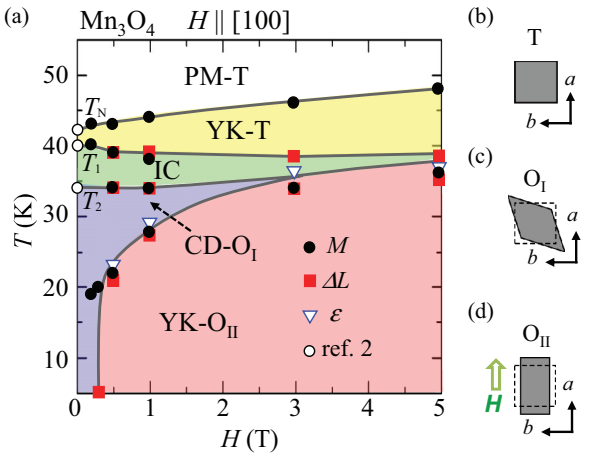

FIG. 3. (Color online) (a) Phase diagram in $H \parallel [100]$. Symbols indicate transition points obtained from the anomalies in Fig. 2. Tetragonal and body-centered-orthorhombic, and face-centered-orthorhombic structures are represented by T, O_I and O_{II}, respectively. (b)–(d) Schematic drawing of (b) T, (c) O_I, and (d) O_{II} structures, respectively. The principal axes in the ab plane are different by 45° between O_I and O_{II} structures.

parallel to H and compressed perpendicular to H, while there is little change along the c axis. The magnitude of the strain approaches up to the order of 10^{-3}, which is huge for a system without orbital degeneracy.

Figure 3(a) shows the obtained phase diagram. Circles (black), rectangles (red), and triangles (blue) denote transition points given by magnetic, strain, and dielectric anomalies in Fig. 2. Phase transition temperatures at 0 T are based on the previous report.[2] In the absence of a magnetic field, there are four phases, PM-T, YK-T, IC, and CD-O_I phases. The T and O_I represent tetragonal and body-centered-orthorhombic structures, respectively, as shown in Figs. 3(b) and 3(c). The crystal system of the IC phase is not obvious yet. Another phase is found to appear at low temperatures in a magnetic field. The magnetic-field-induced phase has a similar magnetic structure to the YK-T phase, while the crystallographic symmetry is not tetragonal, but face-centered-orthorhombic (O_{II}) as discussed later. We thus term the phase YK-type face-centered-orthorhombic (YK-O_{II}) phase. Note that the orthorhombic structures of the YK-O_{II} and the CD-O_I phases are distinct from each other, as shown in Figs. 3(c) and 3(d), where the principal axes in the ab plane are different by 45°. The observed drastic changes in $\Delta\varepsilon/\varepsilon$ and $\Delta L/L$ shown in Figs. 2(b) and 2(c) and anisotropic magnetoelastic response at 5 K in Fig. 2(d) correspond to the phase transition to the YK-O_{II} phase.

B. Crystallographic and magnetic structures

Figures 4(a) and 4(b) show temperature dependence of (0 8 0) reflection profiles of single-crystalline x-ray diffraction in a magnetic field along [100]. The experimental configuration is schematically drawn in Fig. 4(c). After zero-field cooling, a magnetic field was applied up to (a) 1 T or (b) 3 T, and the measurements were performed upon warming. At 10 K, one can see an intense peak indexed as $(0\ 8\ 0)_o$ in addition to a faint peak of (0 8 0) in both 1 T and 3 T. (The subscript o indicates the index in the face-centered orthorhombic setting.) Upon warming, the $(0\ 8\ 0)_o$ peak disappears at 28 K for 1 T and 34 K for 3 T, respectively, and the (0 8 0) peak steeply gains intensity. Comparing the temperatures with those in the phase diagram in Fig. 3(a), the region where the $(0\ 8\ 0)_o$ peak was observed can be assigned to the YK-O_{II} phase. This clearly shows a change in the crystallographic symmetry from

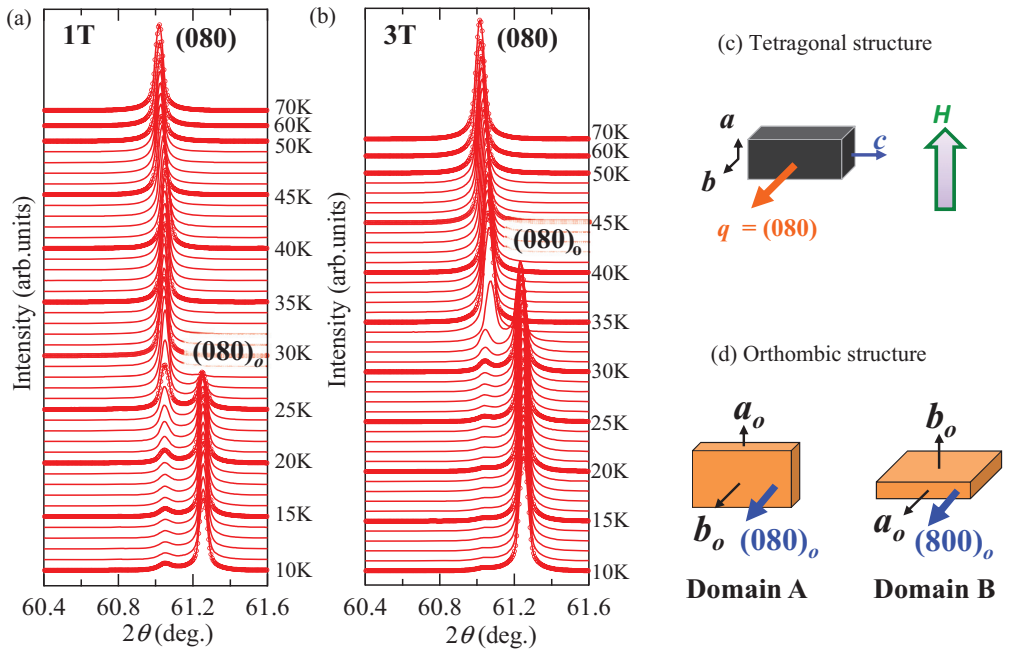

FIG. 4. (Color online) (a) and (b) Temperature dependence of (0 8 0) profiles in a magnetic field of (a) 1 T and (b) 3 T, respectively. The magnetic field is applied ($H \parallel [100]$) perpendicular to both the scattering vector $q \parallel (080)$ and the tetragonal c axis. (d) Two orthorhombic domains corresponding to a tetragonal domain shown in (c). The subscript o indicates the index in orthorhombic setting.

T or O_I to the O_{II} structure in the low temperature region. The presence of the faint (0 8 0) peak indicates that the small amount of the T or the O_I structures coexist in the lowest temperature. As shown in Fig. 4(d), two types of orthorhombic domains A and B could originate from a tetragonal single crystal. In our measurement, these domains are detected by observing $(8\ 0\ 0)_o$ and $(0\ 8\ 0)_o$ reflections, respectively. The extinction of $(8\ 0\ 0)_o$ peak indicates that the application of a magnetic field stabilizes the domain A elongated along H. The obtained lattice constants of the T and the O_{II} phases are $\sqrt{2}a_t = 8.141$ Å and $a_o = 8.114$ Å, respectively. Thus, compressive strain of 0.33% can be induced across the phase transition from T to O_{II} structure. This is in good agreement with the confirmed compressive strain of approximately 0.3% perpendicular to H shown in Fig. 2(d). Therefore, it can be concluded that the magnetic-field-induced anisotropic strain stems from the structural transition from the YK-T or CD-O_I phase to the YK-O_{II} phase, where the longer a axis aligns parallel to H, while the shorter b axis aligns perpendicular to H.

In order to investigate the magnetic structure of the field-induced phase, we carried out a neutron scattering study in a magnetic field. Figure 5(a) shows magnetic-field dependence of neutron scattering profiles at 11 K along $(2+q\ \ -q\ 0)$ and $(0\ q\ 0)$ in the reciprocal space. The profiles were obtained in $H \| [100]$ after zero-field-cooling down to 11 K. At 0 T, two superlattice reflections (1.5 0.5 0) and (2.5 −0.5 0) were observed in addition to fundamental ones (2 0 0) and (0 2 0). The superlattice reflections with a wave vector of $(2\pm q\ -q\ 0)$ $(q = \pm 0.5)$ is characteristic in the CD-O_I phase.[12,13] By applying a magnetic field higher than 0.6 T, the two superlattice reflections disappear, and a fundamental peak (2 0 0) becomes weaker, while the other fundamental peak (0 2 0) becomes stronger. As shown in Fig. 5(c), the abrupt change in these intensities happens at 0.3 T. It corresponds to the phase transition from the CD-O_I to the YK-O_{II} phase, as shown in Fig. 3(a). Therefore, it is considered that the long-wavelength magnetic modulation disappears at the (CD-O_I)-to-(YK-O_{II}) phase transition. We have also performed a synchrotron x-ray diffraction measurement in $H \| [100]$ in order to investigate a superlattice reflection from a lattice modulation. Figure 5(b) shows magnetic-field dependence of synchrotron x-ray profiles at 10 K along $(-0.5\ q\ 0)$ in the reciprocal space. The magnetic field is applied along [100] direction after zero-field-cooling down to 10 K. A superlattice reflection at (−0.5 8.5 0) observed at 0 T disappears above 0.3 T. This shows the presence of a long-wavelength lattice modulation in the CD-O_I phase and the absence in the YK-O_{II} phase. Figure 5(d) shows magnetic-field dependence of the integrated intensity of the (−0.5 8.5 0) superlattice reflection. The H-dependence is similar to the disappearance of the magnetic superlattice [Fig. 5(c)], indicating spin-lattice coupling in Mn_3O_4.

Because of the large tetragonal distortion, we can assume that the AF arrangement of the c axis components in B-site Mn^{3+} spin moments on each chain along [110] and [1$\bar{1}$0] is retained irrespective of the H-induced phase transition. Hence, only the rearrangement of these chains is taken into account. Figures 6(a) and 6(b) show the stacking patterns of 1D-AF chains in the CD-O_I and the YK-O_{II} phases, respectively. Only B-site Mn^{3+} spins projected on to the (0 0 1) plane are

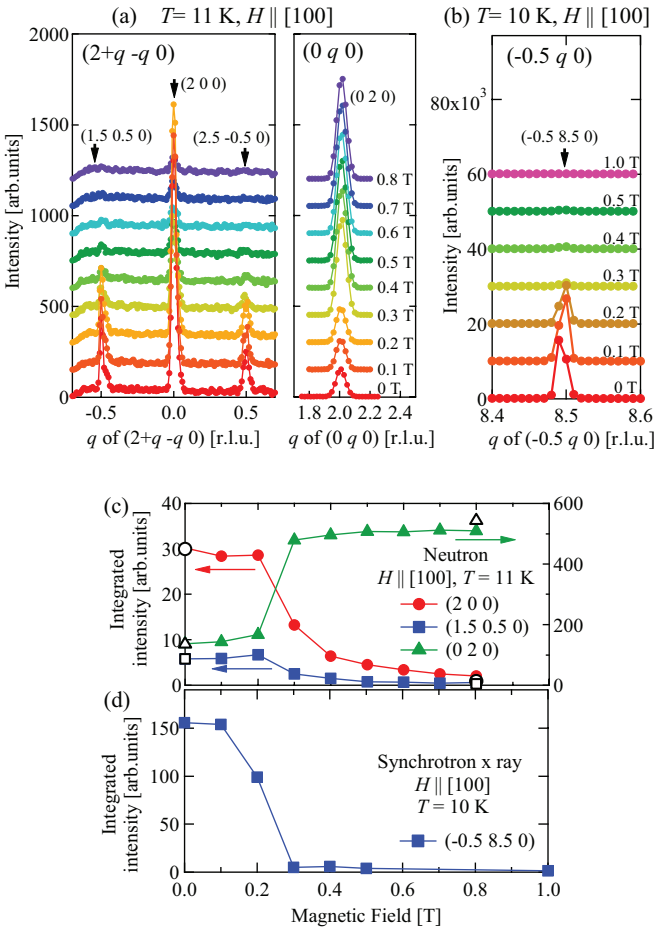

FIG. 5. (Color online) (a) Magnetic-field dependence of neutron magnetic reflections at 11 K. (b) Magnetic-field dependence of (−0.5 8.5 0) superlattice reflection of synchrotron x-ray at 10 K. The magnetic field is applied along [100] in both neutron and synchrotron x-ray diffraction measurements. (c) and (d) The integrated intensities of the magnetic scattering shown in (a) and the (−0.5 8.5 0) superlattice reflection shown in (b) as a function of magnetic field. Open circles, triangles, and rectangles in (c) indicate the calculated intensities of (2 0 0), (0 2 0), and (1.5 0.5 0) reflections for CD-O_I (0 T) and YK-O_{II} phases (0.8 T), respectively (see text).

indicated. The black and white circles indicate up and down spin components along the c axis, respectively. The proposed magnetic structure of the YK-O_{II} phase is characterized as follows: First, the magnetic unit cell is identical to the crystallographic unit cell, consistent with the disappearance of the magnetic superlattice reflections. Second, there is no magnetic modulation parallel to H, while there is a twofold modulation perpendicular to H. This is consistent with a large difference in intensity between (2 0 0) and (0 2 0) magnetic reflections.

Assuming these spin configurations, we have calculated the magnetic scattering intensities. In the calculation, we considered that a multidomain state of CD-O_I structure transforms to the single-domain state of the proposed YK-O_I structure by applying a magnetic field. In Fig. 5(c), the calculations of integrated intensities of these two states are plotted at 0 and 0.8 T, respectively. Excellent agreements between the experimental values and calculations were obtained. It

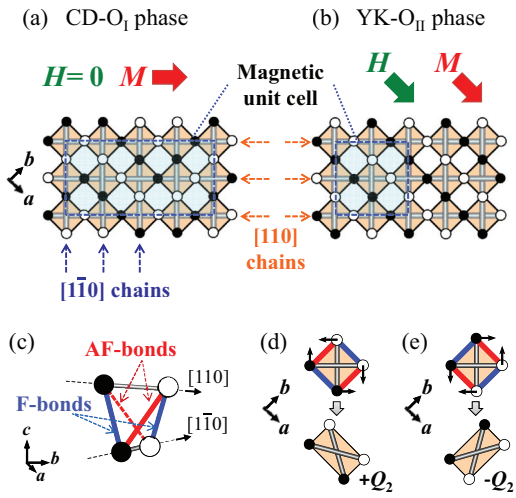

FIG. 6. (Color online) Arrangements of 1D-AF B-site Mn^{3+} chains projected on the (001) plane for (a) the CD-O_I phase and (b) the YK-O_{II} phase, respectively. Black and white circles represent up and down spin components along the tetragonal c axis. (c) A Mn_4 tetrahedron of B sites at the crossing point of two neighboring chains stacked along the c axis. Due to exchange striction between these two chains, AF (F) bonds would become short (long). (d), (e) Orthorhombic distortions of Mn_4 tetrahedra $Q_2 = (\varepsilon_{xx} - \varepsilon_{yy})$. The sign of Q_2 depends on the phases of two relevant 1D-AF chains. The exchange striction mechanism can explain the elongation along H and contraction perpendicular to H when the phase transition from the CD-O_I to the YK-O_{II} takes places.

supports the validity of the proposed change in the stacking pattern of the 1D-AF chains in YK-O_{II} phase. Here, we considered only the rearrangement of the 1D-AF chains, where the magnetic scatterings from only the c axis spin components at the B-site Mn^{3+} were taken into account. In fact, the B-site Mn^{3+} spin moments have the in-plane component, but it has little impact on the scenario for the H-induced phase transition, as discussed later. In order to determine the precise spin configuration including the canting angles, a magnetic structure analysis would be necessary.

Note that the stacking pattern of the 1D-AF chains in the CD-O_I and the YK-O_{II} phases can be converted with each other only by shifting the phases of AF modulation on a half of [1$\bar{1}$0] chains by π. Moreover, the stacking pattern of the YK-O_{II} phase is identical to the YK-T phases. Therefore, phase transitions between CD-type and YK-type magnetic configurations can be considered as the rearrangement in the stacking of 1D-AF chains. On the other hand, the direction of the in-plane component of the YK-O_{II} phase, which is neglected in the discussion above, must be different from the CD-O_I and YK-T phases. The spontaneous magnetization in the CD-O_I and the YK-T phases points toward [110],[12] while the macroscopic magnetization in the YK-O_{II} phase points toward the direction of the applied magnetic field ($H \| [100]$).

The proposed magnetic structure for the YK-O_{II} phase can produce the anisotropic magnetoelastic response through the exchange striction between neighboring B sites.[15] Figure 6(c) shows a Mn_4^{3+} tetrahedron. The direct overlap of t_{2g} orbitals between the top and bottom Mn^{3+} ions, which causes a strong antiferromagnetic exchange interaction, is quite sensitive to the distance between the ions. Therefore, the two AF bonds prefer to be shortened, while the two ferro(F) bonds prefer to be elongated, inducing an orthorhombic distortion of the tetrahedron. Figures 6(d) and 6(e) represent the change in the shape of a Mn_4 tetrahedron via the exchange striction, which can be expressed by the local orthorhombic distortion $Q_2 = (\varepsilon_{xx} - \varepsilon_{yy})$. As shown in Figs. 6(d) and 6(e), the sign of Q_2 just depends on the phases of two relevant chains. In the YK-O_{II} phase, all of the Mn_4 tetrahedra are distorted with the same sign of Q_2 [Fig. 6(d)], resulting in ferro(F) distortion. It can induce lattice elongation parallel to H and compression perpendicular to H. In the CD-O_I phase, on the other hand, there are two kinds of Mn_4 tetrahedra with positive and negative Q_2, which are arranged with the $++--$ configuration along the [110] axis as shown in Fig. 6(a). As a consequence, the local distortions cancel out. Therefore, the magnetic-field-induced anisotropic strain can be understood by the rearrangement in the stacking of 1D-AF chains between the CD-O_I-type to the YK-O_{II}-type, where the exchange striction plays an important role.

C. Spin-lattice coupling in Mn_3O_4

The exchange striction in Mn_3O_4 may produce a long-wavelength lattice modulation coupled with the magnetic one in the CD-O_I phase. As shown in Fig. 5(d), variations of $(-0.5\ 8.5\ 0)$ superlattice reflection directly proves that the long-wavelength lattice modulation is present in the CD-O_I phase, while it is absent in the YK-O_{II} phase. In Fig. 7, the

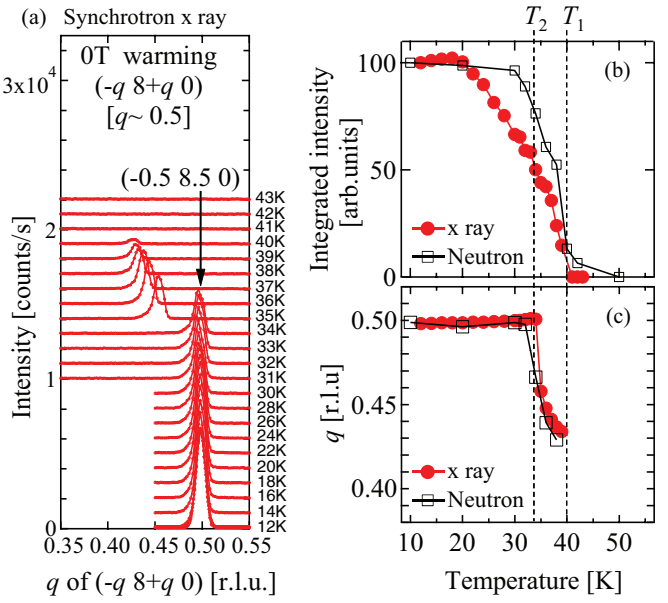

FIG. 7. (Color online) (a) Temperature dependence of profiles of a $(-q\ 8{+}q\ 0)$ ($q \sim 0.5$) superlattice reflection of synchrotron x-ray. The measurement was undertaken upon warming without a magnetic field. (b) and (c) Temperature dependence of the integrated intensities and the propagation vector q of the superlattice reflections shown in (a), in comparison with those of $(2{+}q\ -q\ 0)$ ($q \sim 0.5$) magnetic superlattice reflection obtained by neutron scattering at 0 T. The correspondence indicates a presence of spin-lattice coupling.

spin-lattice coupling is more clearly exhibited. Figure 7(a) shows temperature dependence of profiles of $(-q\ 8{+}q\ 0)$ superlattice reflection at 0 T obtained by using synchrotron x-ray diffraction. The measurement was undertaken upon warming. At low temperatures, a clear superlattice peak at (−0.5 8.5 0) is observed. Upon warming, it shifts to an incommensurate position and then disappears. Figures 7(b) and 7(c) show the temperature dependence of the integrated intensity and the propagation vector q, respectively. It was compared by that of a magnetic superlattice reflection $(2{+}q\ -q\ 0)$ ($q \sim 0.5$) obtained by neutron scattering measurements at 0 T. Both of the superlattice reflections vary in a similar manner: With increasing temperature, the propagation vectors become incommensurate at T_2 and disappear at T_1, corresponding to the phase transitions from the CD-O_I to the IC, and to the YK-T phases, respectively. It is direct evidence that there is a lattice modulation coupled with the magnetic modulation, verifying the presence of spin-lattice coupling caused by the exchange striction between each Mn^{3+} bond.

D. Mechanism of the rearrangement in the stacking of 1D-AF chains

Our results indicate that the magnetic-field-induced phase transition from the CD-O_I to the YK-O_{II} phase should be ascribed to a rearrangement of 1D-AF chains. Here, let us discuss the origin of the chain rearrangements and resultant magnetoelastic and magnetodielectric responses. Figures 8(a) and 8(b) show the magnetic structures for the CD-O_I phase and the YK-O_{II} phase, respectively. The arrow (red) on each Mn_4 tetrahedron characterizes the sign of the local orthorhombic Q_2 distortion. In the CD-O_I phase, two kinds of deformed Mn_4 tetrahedra [Fig. 8(c)] would result in deformations of MnO_6 octahedra with the same modulation vector as the lattice. Figure 8(e) shows two kinds of deformed MnO_6 octahedra, modulated Mn^{3+} hole orbitals, and the in-plane component of the spins for the CD-O_I phase. Once the deformations of MnO_6 octahedra take place, the unoccupied $x^2 - y^2$ orbital should be modified through the electron-lattice coupling. The hole-orbital shape is modulated by a hybridization with $3z^2 - r^2$ orbital as represented by $|\phi_\pm\rangle = \sqrt{1-\delta^2}|x^2-y^2\rangle \pm \delta|3z^2-r^2\rangle$, where δ indicates the degree of hybridization. By considering the electron-lattice coupling, a wave function of $|\phi_+\rangle$ is stabilized in a MnO_6 octahedron with positive Q_2 distortion, while a wave function of $|\phi_-\rangle$ is stabilized in a MnO_6 octahedron with negative Q_2 distortion. Therefore, a long-wavelength orbital modulation should be caused by the lattice deformation. On the other hand, the spin may not contribute to the orbital modulation in the CD-O_I phase.

When a magnetic field is applied along [100] direction at the CD-O_I phase, in-plane component of Mn^{3+} spins rotates from $[\bar{1}\bar{1}0]$ to $[\bar{1}00]$ direction, as represented in Fig. 8(f). This stabilizes the orbital state $|\phi_+\rangle$ through the second-order perturbation of the intratomic spin-orbit coupling at each Mn^{3+} site. As a result, spatial modulation of Mn^{3+} orbitals would disappear and ferro(F) orbital of $|\phi_+\rangle$ state should be realized. This F orbital state favors the F distortion of MnO_6 octahedra and also F distortion of Mn_4 tetrahedra with positive Q_2 through the electron-lattice coupling [Fig. 8(d)]. If we consider the inverse effect of exchange striction, a half of tetrahedra in

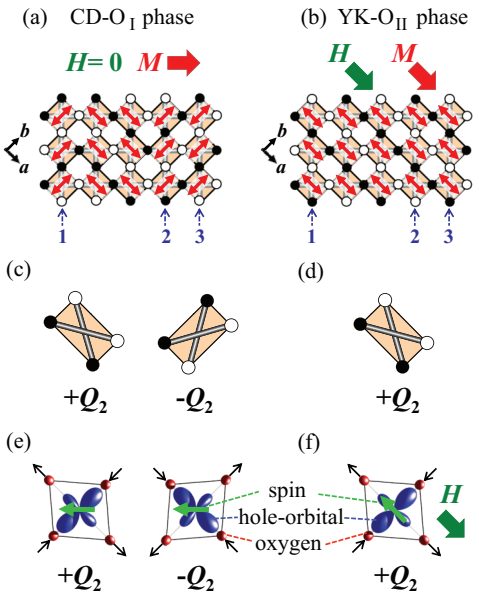

FIG. 8. (Color online) Arrangements of 1D-AF chains with two types of orthorhombic distortions of Mn_4 tetrahedra projected on the c plane for (a) the CD-O_I and (b) the YK-O_{II} phases, respectively. The local distortion of each Mn_4 tetrahedron is characterized by small arrows. Black and white circles indicate up and down spin components of Mn^{3+} ions along the c axis. (c) and (d) Orthorhombically distorted Mn_4 tetrahedra in (c) the CD-O_I and (d) the YK-O_{II} phases, respectively. (e) and (f) Relationship between spin, orbital, and distortion of surrounding octahedron of Mn^{3+} sites in (e) the CD-O_I and (f) the YK-O_{II} phases. Arrows (green) on the Mn^{3+} hole-orbitals represent the in-plane component of the spin. Small arrows (black) beside oxygen atoms show their displacement.

Fig. 8(a) cannot accord with the positive Q_2 distortion. This is because the CD-type magnetic order tends to deform the tetrahedra alternately. Rearrangement of the 1D-AF chains can relax the competition between the spin-orbit-driven lattice distortion and the exchange striction. In the present case, for example, the CD-O_I magnetic structure can be transformed to the YK-O_{II} magnetic structure by shifting the phases of AF modulation on chains 1–3 by π [Figs. 8(a) and 8(b)]. In this scenario, the change in stacking pattern of the 1D-AF chains is caused by the rotation of the in-plane components of Mn^{3+} spins, where the spin-orbit coupling and inverse effect of the exchange striction play a critical role. Here, the anisotropic magnetoelastic response originates from two mechanisms: One is the distortion of MnO_6 octahedra due to the modulation of Mn^{3+} orbital via the spin-orbit coupling, as pointed out by Suzuki *et al.*[3] The other is the exchange striction via the rearrangement of 1D-AF chains, which has not been pointed out so far. Anisotropic magnetodielectric behavior also can be understood as follows. The anisotropic orbital shape results in anisotropic overlap population with oxygen ligands, leading to anisotropic electron hopping. In a site with $|\phi_+\rangle$ shown in Fig. 8(f), for example, the overlap perpendicular to H is larger than that parallel to H. Thus, effective transfer integral perpendicular to H becomes larger than that parallel to H. The anisotropic dielectric response shown in Fig. 2(b) is attributed to the mechanism.

IV. SUMMARY

We have investigated the magnetic-field-induced phase transition of a frustrated tetragonal spinel Mn_3O_4 in $H \parallel [100]$. The phase transition was studied by magnetization, dielectric, and strain measurements, combined with synchrotron x-ray and neutron diffraction. The high-field state is assigned to the face-centered-orthorhombic phase with YK-type magnetic order. The structural phase transition is associated with a rearrangement of frustrated 1D-AF chains composed by B-site Mn^{3+}. We also found a long-wavelength lattice modulation coupled with magnetic modulation, which confirms the presence of spin-lattice coupling caused by the exchange striction between neighboring Mn^{3+} sites. The magnetostructural phase transition in $H \parallel [100]$ is understood in terms of the interplay among spin, orbital, and lattice degrees of freedom. The intratomic spin-orbit coupling and the exchange striction play a critical role in the phase transition.

ACKNOWLEDGMENTS

The authors are grateful to H. Nakao, Y. Yamasaki, and Y. Wakabayashi for their support in synchrotron x-ray diffraction measurements and are also grateful to M. Matsuura for his help in neutron scattering measurements. Y.N. acknowledges a support by a Grant-in-Aid for JSPS Fellows (Grant No. 234410) from the Japan Society for the Promotion of Science. This work was partly supported by a Grant-in-Aid (No. 19052001) from MEXT, Japan.

[1] S. H. Lee, H. Takagi, D. Louga, M. Matsuda, S. Ji, H. Ueda, T. Katsufuji, J. H. Chung, S. Park, S. W. Cheong, and C. Broholm, J. Phys. Soc. Jpn. **79**, 011004 (2010).

[2] R. Tackett, G. Lawes, B. C. Melot, M. Grossman, E. S. Toberer, and R. Seshadri, Phys. Rev. B **76**, 024409 (2007).

[3] T. Suzuki and T. Katsufuji, Phys. Rev. B **77**, 220402(R) (2008).

[4] S. Thota, F. Guillou, V. Hardy, A. Wahl, W. Prellier, and J. Kumar, J. Appl. Phys. **109**, 053902 (2011).

[5] M. Kim, X. M. Chen, Y. I. Joe, E. Fradkin, P. Abbamonte, and S. L. Cooper, Phys. Rev. Lett. **104**, 136402 (2010).

[6] M. Kim, X. M. Chen, X. Wang, C. S. Nelson, R. Budakian, P. Abbamonte, and S. L. Cooper, Phys. Rev. B **84**, 174424 (2011).

[7] J. B. Goodenough and A. L. Loeb, Phys. Rev. **98**, 391 (1955).

[8] K. Dwight and N. Menyuk, Phys. Rev. **119**, 1470 (1960).

[9] B. Mason, Am. Mineral. **32**, 426 (1947).

[10] G. Aminoff, Z. Kristallogr. **64**, 475 (1926).

[11] F. Guillou, S. Thota, W. Prellier, J. Kumar, and V. Hardy, Phys. Rev. B **83**, 094423 (2011).

[12] G. B. Jensen and O. V. Nielsen, J. Phys. C **7**, 409 (1974).

[13] B. Chardon and F. Vigneron, J. Magn. Magn. Mater. **58**, 128 (1986).

[14] J. H. Chung, J. H. Kim, S. H. Lee, T. J. Sato, T. Suzuki, M. Katsumura, and T. Katsufuji, Phys. Rev. B **77**, 054412 (2008).

[15] Recently, it was pointed out that the persistent geometrical frustration in the tetragonal Mn_3O_4 causes a structural instability via spin-lattice coupling, which is related to our scenario. See J. H. Chung, K. H. Lee, Y. S. Song, T. Suzuki, and T. Katsufuji, J. Phys. Soc. Jpn. **82**, 034707 (2013).